

线切割高粗糙度表面的脉冲激光抛光机制研究

姚建华^{1,2}, 黄锦榜^{1,2}, 王光浩^{1,2}, 闵大勇³, 王梁^{1,2*}¹浙江工业大学激光先进制造研究院, 浙江 杭州 310014;²高端激光制造装备省部共建协同创新中心, 浙江 杭州 310014;³苏州长光华芯光电技术有限公司, 江苏 苏州 215000

摘要 在氩气环境下对线切割 316L 不锈钢高粗糙度表面进行脉冲激光抛光实验,通过超景深显微镜拍摄激光抛光前后表面形貌并结合表面划线轮廓和粗糙度值,分析不同脉宽和能量作用形式下抛光表面形貌的演变规律和脉冲激光抛光作用机制。研究结果表明:在相同的单脉冲能量下,随着脉宽增加,表面由原始的“高峰深谷”形貌逐渐演变为“低峰浅谷”形貌,粗糙度由 $R_a=3.79\ \mu\text{m}$ 降至 $R_a=0.95\ \mu\text{m}$,下降 74.9%。激光脉冲能量作用形式逐渐由“低频高能”向“高频低能”转变时,激光作用光斑痕迹逐渐消失,原始表面的峰谷均逐渐减少,激光抛光机制逐渐由“气化”和“熔凝”共同作用的方式转变为单纯的“熔凝”方式。粗糙度降低的最主要原因是激光对表面小凸峰的平滑作用。

关键词 激光技术; 激光材料加工; 脉冲激光; 激光抛光; 表面形貌; 表面粗糙度

中图分类号 TN249; TG665

文献标志码 A

doi: 10.3788/CJL202148.1402003

1 引言

电火花线切割适用于各类外形轮廓不规则金属零件的切割成形^[1],其快走丝的加工形式相较慢走丝具有成本低和效率高的优势,但线切割后的表面粗糙度值较大,一般为 $R_a=3\sim 6\ \mu\text{m}$ ^[2]。对于线切割后外形轮廓不规则的工件,现有的抛光方式主要有机械抛光、化学抛光、电化学抛光等。然而,以上传统抛光方式存在着效率相对较低、人工劳动强度大、环境污染和不规则零件难以抛光等缺点。激光抛光是激光加工技术发展过程中出现的一种新型的表面处理技术,具有高效率、无污染、可选区抛光以及可抛光不规则几何表面等诸多优点^[3-5],能避免上述传统抛光方式的缺点。

激光抛光主要有脉冲激光抛光和连续激光抛光两种形式。前者被称为激光微观抛光(laser micro-polishing),通常针对的是原始粗糙度为 $R_a=0.2\sim 1\ \mu\text{m}$ 的表面;后者被称为激光宏观抛光(laser macro-polishing),通常针对的是原始粗糙度 $R_a=$

$2\sim 16\ \mu\text{m}$ 的表面^[6]。通常可将待抛光表面的粗糙度等级大致分为高粗糙度($R_a=2\sim 16\ \mu\text{m}$)、中等粗糙度($R_a=1\sim 2\ \mu\text{m}$)、低粗糙度($R_a<1\ \mu\text{m}$)。

目前,国内外学者已针对模具钢、不锈钢、钛合金等金属材料进行了大量的激光抛光研究,并获得了较好的抛光效果,如:杨奇彪等^[7]在低粗糙度($R_a=0.23\ \mu\text{m}$)的 Ti6Al4V 表面上采用波长为 1064 nm 的纳秒脉冲光纤激光进行了抛光实验,结果发现,脉冲能量密度、脉宽、光斑重叠率增大,表面粗糙度均减小,但重叠率过大反而会增加粗糙度;Ma 等^[8]研究了波长为 1070 nm 的脉冲光纤激光抛光低粗糙度($R_a=0.21\ \mu\text{m}$)Ti6Al4V 时的熔池流动和表面演变,发现马兰戈尼流效应随脉宽增大而增强;Nüsser 等^[9]采用波长为 1064 nm 的脉冲光纤激光器对低粗糙度($R_a=0.11\ \mu\text{m}$)的工具钢表面进行了激光抛光,结果发现,短脉宽无法维持熔体流动,只能降低表面小范围内的粗糙度,而长脉宽因更易使熔体保持流动而降低了表面大范围内的粗糙度;Dai 等^[10]利用波长为 1070 nm 的多模连续光纤激

收稿日期: 2020-11-03; 修回日期: 2020-12-15; 录用日期: 2021-01-11

基金项目: 国家自然科学基金(52035014)

通信作者: *ddtwl@foxmail.com

光器将线切割 SKD11 工具钢的表面粗糙度由原始的高粗糙度 ($R_a = 3.59 \mu\text{m}$) 降至低粗糙度 ($R_a = 0.473 \mu\text{m}$), 并发现随着激光能量密度增加, 表面经历了浅熔到深熔的变化; 周泳全等^[11]对冷作模具钢进行连续激光抛光后发现, 采用平顶光斑并优化扫描路径能将较高粗糙度 (R_a 约为 $2.0 \mu\text{m}$) 的表面快速抛光至与机械磨削加工相同的表面粗糙度范围 ($R_a = 0.2 \sim 0.8 \mu\text{m}$); Chen 等^[12]采用皮秒脉冲激光器对低粗糙度 ($R_a = 0.22 \mu\text{m}$) 的 ASP23 钢表面进行了激光微观抛光实验, 结果发现采用皮秒激光能明显降低工件的热变形, 但效率较纳秒激光抛光低, 只适用于低粗糙度表面精度的进一步提升。

针对增材制造的 316L 不锈钢高粗糙度表面, Obeidi 等^[13]采用波长为 $10.6 \mu\text{m}$ 的 CO_2 连续激光将其表面粗糙度由 $R_a = 10.4 \mu\text{m}$ (高粗糙度) 降至 $R_a = 2.7 \mu\text{m}$, 且未发现相变和硬度改变。Rosa 等^[14]采用连续光纤激光将铣削工件的表面粗糙度由 $R_a = 13.6 \mu\text{m}$ (高粗糙度) 降至 $R_a = 0.93 \mu\text{m}$, 并发现原始形貌和激光参数会影响最终的形貌。针对砂纸打磨的 316L 不锈钢低粗糙度表面, 张峰烈等^[15]采用波长为 355 nm 的紫外脉冲激光将其表面粗糙度由 $R_a = 195.82 \text{ nm}$ 降至 146.59 nm , 并发现相同脉冲能量密度下存在最佳的扫描速度和离焦距离。由上述研究可以发现, 目前脉冲激光对高粗糙度表面的抛光及其作用机制尚未有详细研究。鉴于

此, 本文对快走丝线切割 316L 不锈钢高粗糙度表面进行脉冲激光抛光, 然后用超景深显微镜观察抛光前后表面的三维微观形貌, 测量表面轮廓和粗糙度值, 分析不同激光脉宽和能量作用形式下抛光表面形貌的演变规律以及脉冲激光抛光高粗糙度表面的作用机制。

2 抛光实验及表面形貌、粗糙度测试

实验材料为 316L 奥氏体不锈钢。实验前, 用型号为 DK77-30 的电火花数控线切割机床切出高粗糙度表面, 切割参数如下: 放电电压 80 V , 放电电流 3 A , 脉宽 $40 \mu\text{s}$, 脉冲间隔 $400 \mu\text{s}$, 钼丝直径 0.18 mm 。然后对粗糙表面进行超声清洗, 最后进行干燥处理。测量后, 得到试样的表面粗糙度为 $R_a = 3.79 \mu\text{m}$, 其表面形貌如图 1(a) 所示。

脉冲激光抛光实验设备如图 1(b) 所示。采用 MOPA 型纳秒脉冲激光器进行抛光实验, 该激光器的最大平均功率为 100 W , 激光波长为 1064 nm , 聚焦光斑直径为 $100 \mu\text{m}$ 。为防止激光抛光过程中材料表面氧化, 将工件置于气氛保护箱内。实验前采用“下进上出”的方式通气 5 min , 以排除箱内空气, 且在激光抛光实验过程中持续通入高纯氩气, 氩气流量为 15 L/min 。激光通过透镜对工件表面进行抛光。激光抛光采用“弓”字形扫描填充方式。扫描区域尺寸为 $10 \text{ mm} \times 10 \text{ mm}$, 线间距设定为 $50 \mu\text{m}$ 。

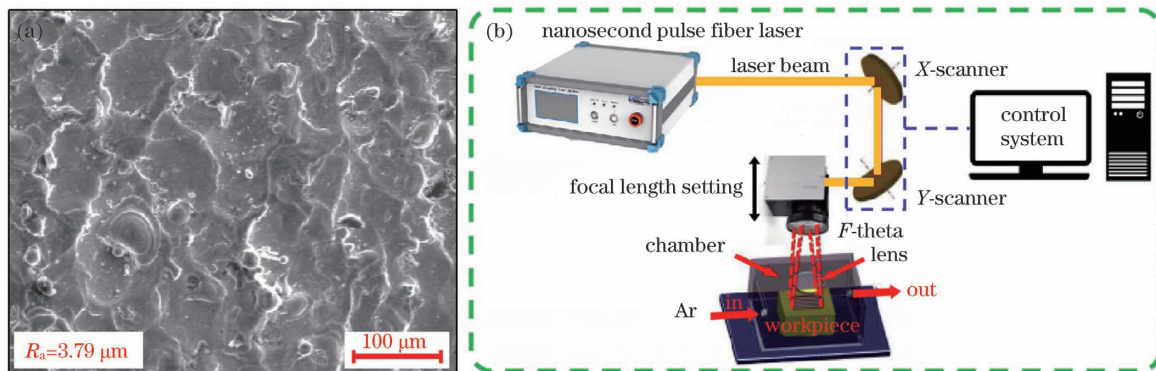


图 1 试样表面形貌及实验设备示意图。(a)电火花线切割表面;(b)实验设备示意图

Fig. 1 Surface morphology of sample and schematic of laser-polishing setup. (a) Surface cut by wire electrical discharge machining; (b) schematic of experimental equipment

采用 NIKON 体视显微镜和基恩士 VHX-5000 超景深显微镜分别对抛光表面的宏观形貌和微观形貌进行观察分析。采用 TR-130A 粗糙度仪检测试样的表面粗糙度。

3 结果与讨论

3.1 MOPA 激光抛光参数的选择与抛光宏观形貌

脉宽不同的 MOPA 激光器具有不同的截止频

率和最大单脉冲能量^[16]。为研究脉宽对抛光表面形貌的影响,设定激光平均功率为 100 W,重复频率为 500 kHz,固定单脉冲能量为 0.2 mJ;同时,为了提高激光抛光效率,扫描速度设定为 1000 mm/s,

扫描区域填充线间距(d)设定为 0.05 mm。最后设定不同的脉宽(10, 50, 150, 250, 350 ns 进行激光抛光实验,同区域扫描 4 次,具体的激光抛光实验参数如表 1 所示。

表 1 不同脉宽下的激光抛光参数

Table 1 Laser polishing parameters at different pulse duration values

No.	Power /W	Velocity / (mm · s ⁻¹)	Pulse duration /ns	Repetition frequency /kHz	Step size /mm	Pulse energy / mJ
A1	100	1000	10	500	0.05	0.2
A2	100	1000	50	500	0.05	0.2
A3	100	1000	150	500	0.05	0.2
A4	100	1000	250	500	0.05	0.2
A5	100	1000	350	500	0.05	0.2

为研究脉冲能量作用形式对抛光表面形貌的影响,设定激光平均功率 P 为 100 W,脉宽 ω 为 400 ns(如表 2 所示),以达到最高的单脉冲能量 E 。通过改变重复频率来改变单脉冲所具有的能量,但重复频率 f 与扫描速度 v 两者共同决定着扫描过程中的光斑叠加率^[17],固定扫描速度会带来不同的光斑叠加率,因此提出了不同能量作用形式的脉冲

激光抛光概念。随着重复频率由 66 kHz 升至 1000 kHz,单脉冲能量逐渐降低,光斑叠加率分别为 78%、86%、93%和 99%,脉冲能量作用形式从“高频低能”向“低频高能”转变,即激光从低频分散脉冲逐渐向高频类连续激光转变。

采用体视显微镜拍摄不同脉宽和不同能量作用形式下的激光抛光表面形貌,宏观形貌如图 2 所示。

表 2 不同脉冲能量作用形式下的激光抛光参数

Table 2 Laser polishing parameters in different pulse energy forms

No.	Power /W	Velocity / (mm · s ⁻¹)	Pulse duration /ns	Repetition frequency /kHz	Step size /mm	Pulse energy / mJ
B1	100	1000	400	66	0.05	1.5
B2	100	1000	400	100	0.05	1.0
B3	100	1000	400	200	0.05	0.5
B4	100	1000	400	1000	0.05	0.1

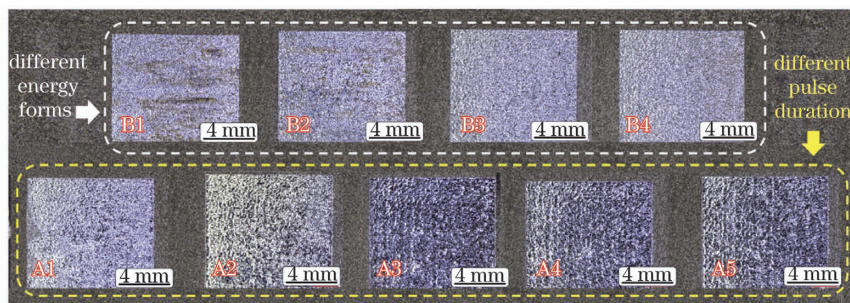


图 2 体视显微镜拍摄的不同脉宽和能量作用形式下抛光表面的宏观照片

Fig. 2 Pictures of polished surface in different pulse duration values and pulse energy forms photographed by stereo microscope

3.2 脉冲宽度对表面形貌的影响规律

超景深显微镜拍摄的不同脉宽下激光抛光后的三维表面轮廓如图 3 所示,抛光表面划线部位的轮廓如图 4 所示。对比图 3 作用区域与原始区域可以发现,不同的脉宽参数都能对高粗糙度表面起到平

滑作用,且微观表面的峰部均得到平滑,这是因为激光首先接触到的是粗糙表面的凸出部位。

激光脉宽为 10 ns 时的表面形貌如图 3(a)所示,表面的微观峰部在激光作用后变得平滑,但表面依旧残留有较多的原始凹陷谷部。激光脉宽为

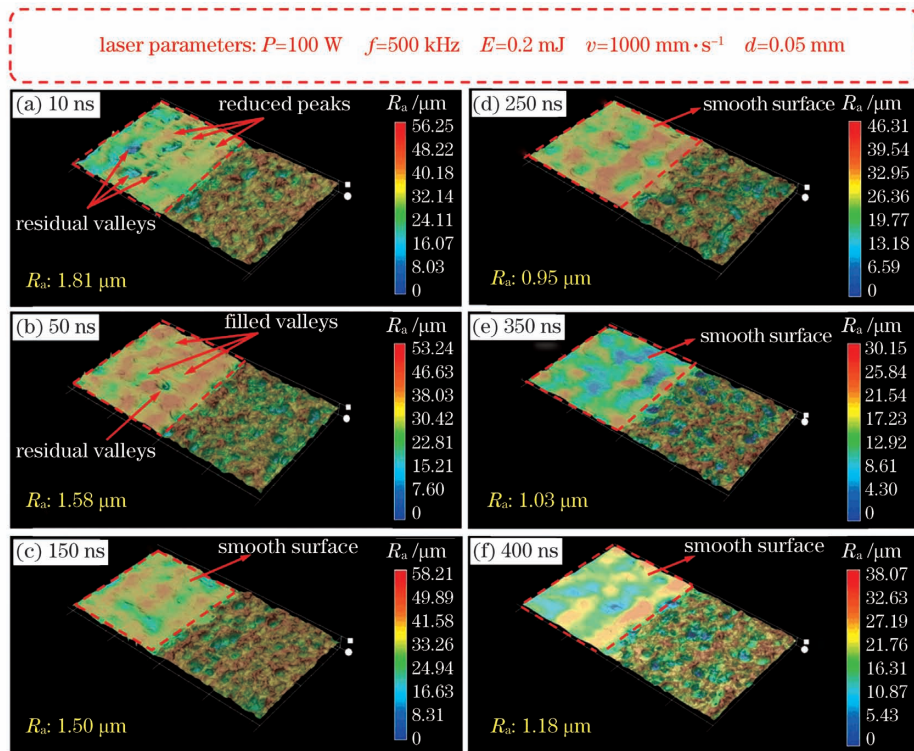


图 3 不同脉宽下抛光表面形貌的演变。(a) 10 ns; (b) 50 ns; (c) 150 ns; (d) 250 ns; (e) 350 ns; (f) 400 ns
 Fig. 3 Evolution of surface morphologies in different pulse duration values. (a) 10 ns; (b) 50 ns; (c) 150 ns; (d) 250 ns; (e) 350 ns; (f) 400 ns

50 ns 时的表面形貌如图 3(b) 所示, 残留的原始凹陷谷部数量减少, 仅存少量深谷。随着脉宽进一步增加, 抛光后的形貌开始趋于一致, 峰部与谷部数量均减少, 如图 3(c~f) 所示。

图 4 为不同脉宽激光抛光表面的划线部位及其对应的轮廓。原始线切割表面由于电火花放电爆炸而具有不规则的峰、谷形状, 谷部形状为放电造成的类“陨石坑”形状, 而峰部则处于谷与谷之间, 通常又窄又尖。由图 4(a) 所示的表面轮廓线可知, 在

10 ns 脉宽下, 窄尖状高峰降低, 但放电造成的类“陨石坑”形貌并未完全消失, 这与图 3(a) 所示的三维轮廓结果相对应, 表面几乎无原始凸起的高峰, 但存在残留谷部。在 50 ns 脉宽下, 谷部数量进一步减少, 见图 4(b)。当脉宽为 150 ns 时, 表面划线轮廓的峰部和谷部均趋于平坦, 如图 4(c) 所示。当脉宽分别为 250, 350, 400 ns 时, 表面划线轮廓不存在尖锐的峰部和谷部, 而是一条接近平缓、略有起伏的表面轮廓曲线, 但并不是严格意义上的水平线, 如图 4(g) 所示。

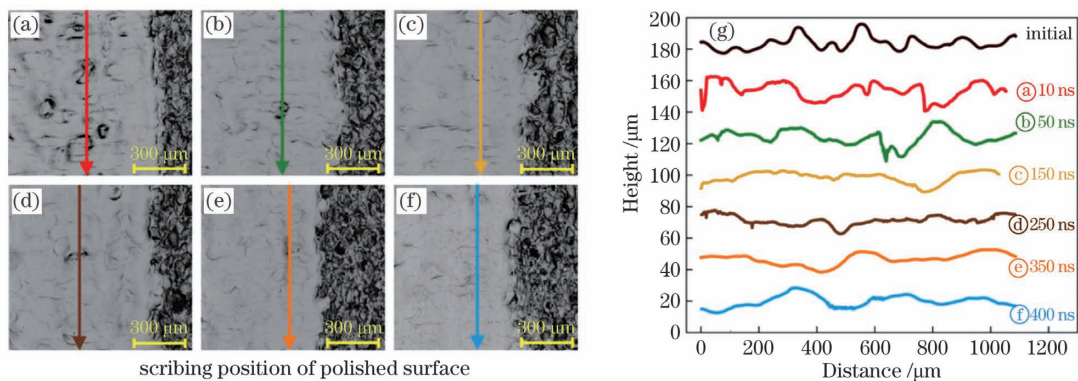


图 4 不同脉宽抛光表面划线部位及其轮廓。(a) 10 ns; (b) 50 ns; (c) 150 ns; (d) 250 ns; (e) 350 ns; (f) 400 ns; (g) 轮廓
 Fig. 4 Scribing positions and profiles of polished surface in different pulse duration values. (a) 10 ns; (b) 50 ns; (c) 150 ns; (d) 250 ns; (e) 350 ns; (f) 400 ns; (g) profiles

3.3 脉冲能量形式对表面形貌的影响规律

不同脉冲能量形式下的三维表面轮廓如图 5 所示,抛光表面划线部位及其轮廓如图 6 所示,可以发现,不同脉冲能量对表面形貌产生了明显不同的作用。当脉冲能量为 1.5 mJ、光斑重叠率为 78% 时,脉冲能量形式更接近脉冲形式,作用后的表面形貌如图 5(b) 所示,线切割峰部平滑,残留有大量谷部。这是因为高能激光束使表面薄层材料气化产生等离子体,等离子体遮蔽后续脉冲激光束,影响了其对谷部的作用,导致仅有少量谷部受激光作用而变得平缓,而大部分谷部都保留下来。从图 5(b) 区域①中的表面形貌放大图可以看出,高能脉冲激光在表面

产生了光斑作用的边缘痕迹,痕迹极其微小(起伏 3~5 μm),因此气化冲击也极其微小。当单脉冲能量减至 1.0 mJ、光斑重叠率为 86% 时,表面形貌如图 5(c) 所示,放大部分如图 5(c) 区域②所示,脉冲能量降低,光斑边缘无法气化,因此没有出现图 5(b) 区域①所示的光斑作用的边缘痕迹,表面主要发生瞬时熔凝,仅有少量气化,更高的重叠率使谷部作用时间更长,减少了谷部的残留。随着单脉冲能量进一步降低和光斑重叠率进一步上升,整体表面形貌如图 5(d)、(e) 所示,从图 5(d) 区域③和图 5(e) 区域④的表面形貌放大图可以看出,谷部得以填充,表面形貌趋于一致。

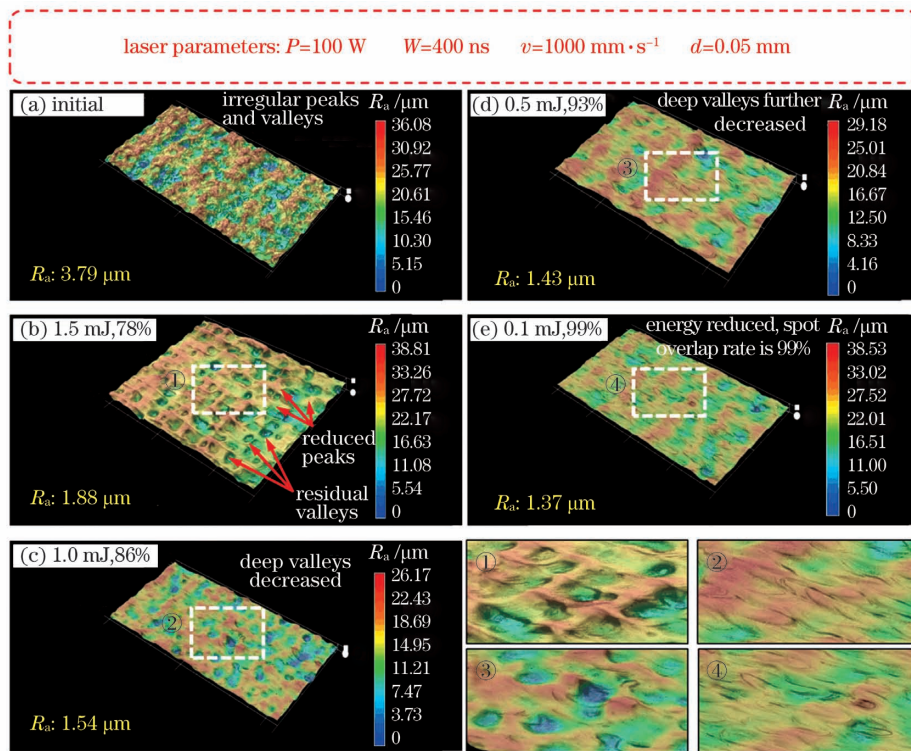


图 5 不同脉冲能量及光斑重叠率下抛光表面的形貌。(a)原始形貌;(b)脉冲能量 1.5 mJ,光斑重叠率 78%;(c)脉冲能量 1.0 mJ,光斑重叠率 86%;(d)脉冲能量 0.5 mJ,光斑重叠率 93%;(e)脉冲能量 0.1 mJ,光斑重叠率 99%

Fig. 5 Morphologies of polished surface at different pulse energy value and spot overlap rates. (a) Initial morphology; (b) pulse energy of 1.5 mJ, spot overlap rate of 78%; (c) pulse energy of 1.0 mJ, spot overlap rate of 86%; (d) pulse energy of 0.5 mJ, spot overlap rate of 93%; (e) pulse energy of 0.1 mJ, spot overlap rate of 99%

图 6 为不同脉冲能量形式下抛光表面划线部位及其轮廓。由表面划线轮廓的变化可以看出,在“低频高能”的能量形式下,表面尖峰区域被削短,谷部存在残留。随着单脉冲能量的降低以及光斑重叠率的增大,表面峰部降低,同时谷部数量减少,主要发

生熔凝作用,即“熔峰填谷”^[18]。最终,当单脉冲能量为 0.1 mJ、光斑叠加率为 99% 时,表面轮廓相较于线切割轮廓更加平缓。这是因为此时的光斑重叠率极高,即光斑在相同的位置不断熔化凝固表面,以 1% 的间隙逐步推进,最终获得了更为平缓的表面。

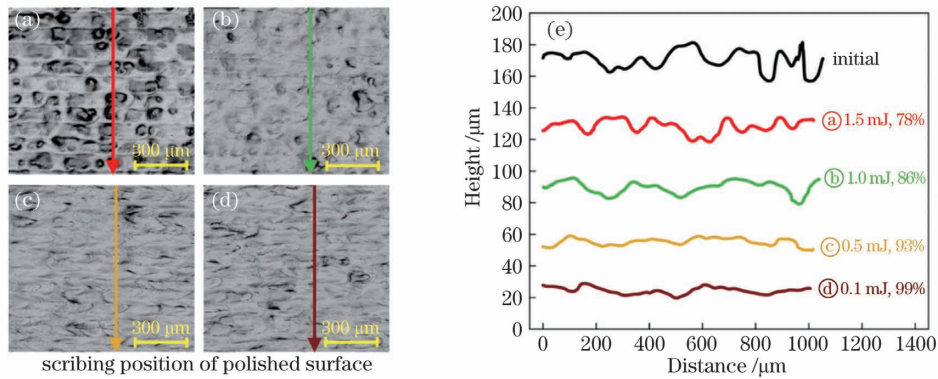


图 6 不同脉冲能量及光斑重叠率下抛光表面的划线部位及其轮廓。(a) 脉冲能量 1.5 mJ, 光斑重叠率 78%; (b) 脉冲能量 1.0 mJ, 光斑重叠率 86%; (c) 脉冲能量 0.5 mJ, 光斑重叠率 93%; (d) 脉冲能量 0.1 mJ, 光斑重叠率 99%; (e) 轮廓

Fig. 6 Scribing positions and profiles of polished surface at different pulse energy values and spot overlap rates. (a) Pulse energy of 1.5 mJ, spot overlap rate of 78%; (b) pulse energy of 1.0 mJ, spot overlap rate of 86%; (c) pulse energy of 0.5 mJ, spot overlap rate of 93%; (d) pulse energy of 0.1 mJ, spot overlap rate of 99%; (e) profiles

3.4 脉宽和脉冲能量形式对表面粗糙度的影响规律

线切割表面的粗糙度为 $R_a = 3.79 \mu\text{m}$, 脉冲激光抛光后粗糙度最低降至 $R_a = 0.95 \mu\text{m}$, 降幅达 74.9%。表面粗糙度 R_a 随脉宽的变化趋势如图 7(a) 所示, 不同的脉宽均具有大幅降低表面粗糙度的作用。随着脉宽增加, 熔化凝固持续时间增加, 因此更能平缓凹凸不平的表面, 表面粗糙度 R_a 逐渐减小并最终趋于饱和。表面粗糙度最终趋于饱和无法再降低是由于脉冲激光仅在极短的时间内作用于表面浅层, 能量难以向材料内部传输, 因此对于高

粗糙度表面, 表面的大范围起伏现象难以消除, 阻碍了粗糙度的进一步降低。

表面粗糙度值 R_a 随不同脉冲能量形式的变化趋势如图 7(b) 所示, 随着能量形式从“低频高能”向“高频低能”转变, 粗糙度逐渐降低, 最低达 $R_a = 1.37 \mu\text{m}$, 降幅为 69.4%, 同样具有大幅降低原始表面粗糙度的作用。“高频低能”的脉冲能量形式因为近似于类连续激光的作用方式而使表面具有更佳的粗糙度值, 这与 Krishnan 等^[6] 提出的连续激光更适合于高粗糙度表面抛光而脉冲激光更适合于低粗糙度表面抛光的结论相符合。

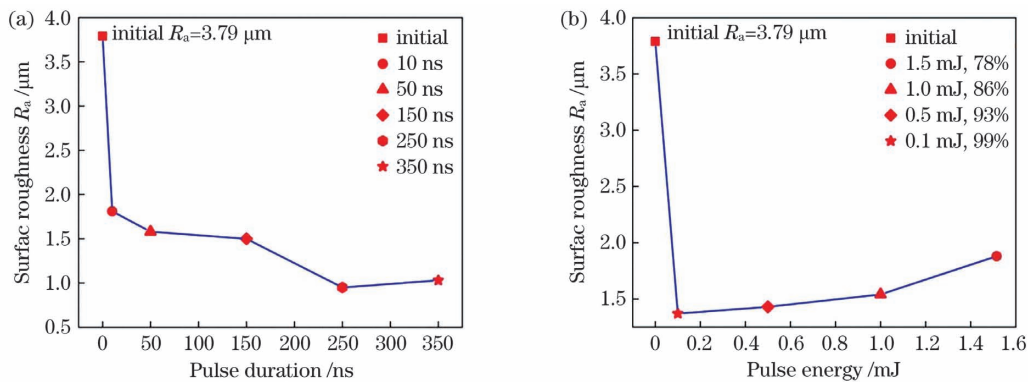


图 7 不同脉宽和脉冲能量形式下表面粗糙度 R_a 的变化。(a) 表面粗糙度随脉宽的变化; (b) 表面粗糙度随脉冲能量及光斑重叠率的变化

Fig. 7 Variations of surface roughness R_a at different pulse duration and pulse energy forms. (a) Variation of surface roughness with pulse duration; (b) variation of surface roughness with pulse energy and spot overlap rate

3.5 脉冲激光抛光机理

为了进一步探究脉冲激光对高粗糙表面微观峰部和谷部的作用机理, 设置不同的能量作用形式进行单道实验, 利用超景深显微镜观察激光作用区域微观峰部和谷部的变化。

图 8 为“低频高能”能量作用形式(单脉冲能量 1.5 mJ, 光斑重叠率 78%) 下单道的超景深三维表面地貌及表面划线轮廓。为研究激光对高粗糙表面浅峰、浅谷、深谷三个表面特征的影响, 选取包含以上三种特征的 A、B 两线为截取线, 输出表面划线的

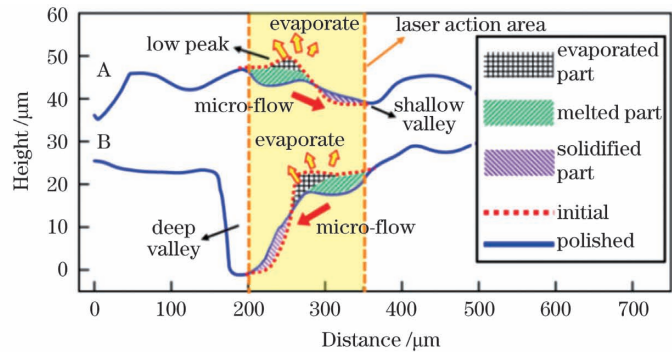
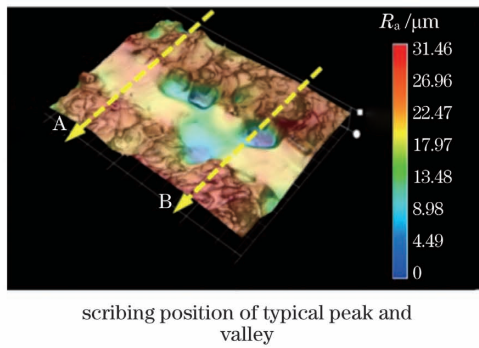


图 8 “低频高能”形式脉冲激光对高粗糙度表面微观峰部和谷部的作用。(a)三维表面形貌;(b)表面划线轮廓
Fig. 8 Effects of high energy dispersion pulse laser on micro peak and valley of high roughness surface.

(a) Three-dimensional surface morphology; (b) profiles of surface scribing

轮廓。如图 8 中 A 处划线轮廓所示,当激光作用于低峰和浅谷时,低峰凸出部位发生材料气化。这是因为呈高斯分布的激光束中心能量高,以窄小为特征的低峰处于光斑中心更易气化,而中心至边缘过渡区域的材料熔化流动,该现象与 Guo 等^[19]采用脉冲激光对 DF-2 冷作模具钢进行抛光时所发现的当输入的热量 (H_{input}) 大于金属的熔化热阈值 ($H_{threshold}$) 时,主要作用机制为金属的蒸发和熔化相类似。在重力作用下,处于较高处(低峰处)的熔体部分发生微流动,最终在低处(浅谷处)凝固,但这种熔化流动存在的时间极短且不稳定,故无法使表面充分平坦化。如图 8 中 B 处划线轮廓所示,当激光作用于深谷时,深谷边缘凸出部位因处于光斑中心而产生气化,其他区域的材料熔化后在重力作用下向深谷流动迁移,但无法持续稳定流动,最终于深谷侧面凝固。以上结果表明,“低频高能”的脉冲能量作用形式对低峰、浅谷的平坦化相较深谷具有更佳的效果,从“低频

高能”的脉冲能量作用形式对深谷的作用结果亦可以看出,该种形式的激光脉冲缺乏持续的热量输入,熔体无法持续稳定流动,无法填充深谷。

图 9 为“高频低能”作用形式下单道超景深三维表面形貌及表面划线轮廓,选取包含浅峰、深谷两种特征的 A、B 两线为截取线,输出表面划线轮廓。如图 9 中 A 处划线轮廓所示,当激光作用于深谷特征部位时,在 0.1 mJ 的单脉冲能量下,作用区域无气化现象发生,但 99% 的光斑重叠率使表面具有持续的热量输入,材料熔化流动的时间更长久,最终实现了深谷的填充。如图 9 中 B 处划线轮廓所示,当激光作用于浅峰特征部位时,作用机制与前者相同,中心较高处熔化的材料在重力作用下向周围流动,表面趋于平整。以上现象与 Liu 等^[20]采用 500 kHz 高重复频率、1000 mm/s 扫描速度、2 μ m 线间距对 5A06 铝合金进行激光抛光时所发现的凝固区域会再次熔化流动且熔池持续时间更长的现象相吻合。

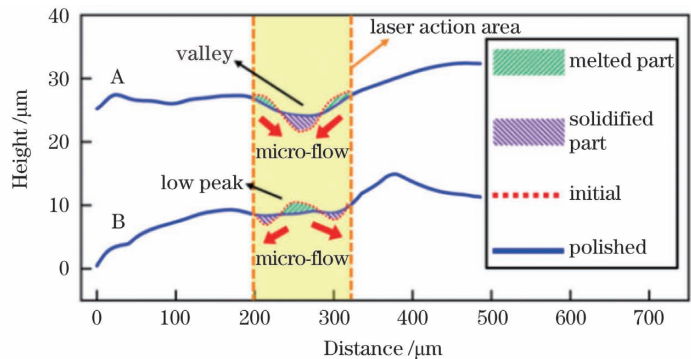
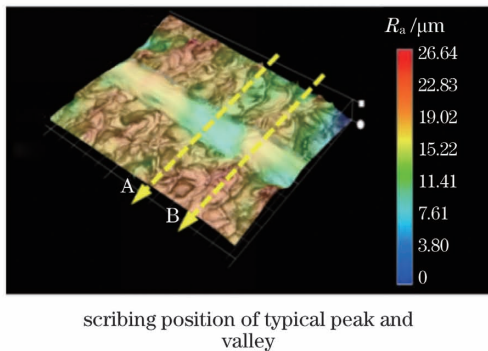


图 9 “高频低能”形式脉冲激光对高粗糙度表面微观峰部和谷部的作用。(a)三维表面形貌;(b)表面划线轮廓
Fig. 9 Effect of low energy concentration pulse laser on micro peak and valley of high roughness surface.

(a) Three-dimensional surface morphology; (b) profiles of surface scribing

4 结 论

本文采用脉宽和重复频率大范围可调节的

MOPA 脉冲激光来抛光线切割高粗糙度表面,分析了不同脉宽和不同脉冲能量作用形式下抛光表面轮廓的三维形貌、划线轮廓及表面粗糙度,得出以下

结论:

1)保持其他激光参数不变,不同脉宽下微观表面的峰部均会降低,而谷部则随着脉宽的增加表现出逐渐填充的趋势,表面粗糙度降低并最终达到饱和状态,由原始的 $R_a = 3.79 \mu\text{m}$ 降至 $R_a = 0.95 \mu\text{m}$,降幅达 74.9%。

2)保持其他脉冲激光参数不变,脉冲能量形式由“低频高能”向“高频低能”转变,表面光斑作用痕迹逐渐消失,峰部降低而谷部逐渐填充,表面粗糙度由原始的 $R_a = 3.79 \mu\text{m}$ 降至 $R_a = 1.37 \mu\text{m}$,降幅达 69.4%。

3)在不同的脉冲能量形式下,当以脉冲抛光方式逐渐向类连续抛光方式转变时,表面逐渐由气化熔化并行抛光向单纯熔凝抛光演变,熔凝抛光更适合于高粗糙度表面的抛光。

4)脉冲激光抛光降低表面粗糙度的最主要原因在于光斑对表面窄小凸峰的平滑作用。原始高粗糙度表面所具有的宏观起伏无法整体平缓,这是限制脉冲激光抛光高粗糙度表面时粗糙度进一步下降的原因。

参 考 文 献

- [1] Song L J. Effects on damaged layers of the process parameters of wire electrical discharge machining in high carbon martensitic stainless steel[D]. Shanghai: Shanghai Jiao Tong University, 2015: 1-8.
宋良杰. 电火花线切割工艺参数对高碳马氏体不锈钢变质层的影响[D]. 上海: 上海交通大学, 2015: 1-8.
- [2] Kumar R, Roy S, Gunjan P, et al. Analysis of MRR and surface roughness in machining Ti-6Al-4V ELI titanium alloy using EDM process [J]. Procedia Manufacturing, 2018, 20: 358-364.
- [3] Chen L, Yang Y Q. Mechanism and application of laser polishing [J]. Surface Technology, 2003, 32(5): 49-52.
陈林, 杨永强. 激光抛光机理及应用[J]. 表面技术, 2003, 32(5): 49-52.
- [4] Dai W, Zheng Z Z, Li J J, et al. Research progress of laser polishing on the metal surface [J]. Laser & Optoelectronics Progress, 2015, 52(11): 110001.
戴伟, 郑志镇, 李建军, 等. 金属材料表面的激光抛光研究进展 [J]. 激光与光电子学进展, 2015, 52(11): 110001.
- [5] Lamikiz A, Sanchez J A, de Lacalle L N L, et al. Laser polishing techniques for roughness improvement on metallic surfaces [J]. International Journal of Nanomanufacturing, 2007, 1(4): 490.
- [6] Krishnan A, Fang F Z. Review on mechanism and process of surface polishing using lasers [J]. Frontiers of Mechanical Engineering, 2019, 14(3): 299-319.
- [7] Yang Q B, Wang H J, Huang Y, et al. Experimental study on nanosecond laser polishing of Ti6Al4V alloy [J]. Optical Technique, 2019, 45(2): 245-250.
杨奇彪, 王昊君, 黄易, 等. 纳秒激光抛光钛合金 Ti6Al4V 作用机理的实验研究 [J]. 光学技术, 2019, 45(2): 245-250.
- [8] Ma C, Vadali M, Duffie N A, et al. Melt pool flow and surface evolution during pulsed laser micro polishing of Ti6Al4V [J]. Journal of Manufacturing Science and Engineering, 2013, 135(6): 061023.
- [9] Nüsser C, Wehrmann I, Willenborg E. Influence of intensity distribution and pulse duration on laser micro polishing [J]. Physics Procedia, 2011, 12: 462-471.
- [10] Dai W, Li J J, Zhang W K, et al. Evaluation of fluences and surface characteristics in laser polishing SKD 11 tool steel [J]. Journal of Materials Processing Technology, 2019, 273: 116241.
- [11] Zhou Y Q, Zhang W, Xiao H B, et al. Roughness and property of CW laser high speed polishing of die steel [J]. Surface Technology, 2020, 49(2): 347-353.
周泳全, 张卫, 肖海兵, 等. 连续激光高速抛光冷作模具钢的表面粗糙度及性能 [J]. 表面技术, 2020, 49(2): 347-353.
- [12] Chen Y D, Tsai W J, Liu S H, et al. Picosecond laser pulse polishing of ASP23 steel [J]. Optics & Laser Technology, 2018, 107: 180-185.
- [13] Obeidi M, McCarthy E, O'Connell B, et al. Laser polishing of additive manufactured 316L stainless steel synthesized by selective laser melting [J]. Materials, 2019, 12(6): 991.
- [14] Rosa B, Hascoët J Y, Mognol P. Topography modeling of laser polishing on AISI 316L milled surfaces [J]. Mechanics & Industry, 2014, 15(1): 51-61.
- [15] Zhang F L, Fu X, Liu C Y. Influences of nanosecond pulsed laser on parameters in micro-polishing of stainless steel 316L [J]. Nanotechnology and Precision Engineering, 2011, 9(4): 370-376.
张峰烈, 傅星, 刘春阳. 纳秒脉冲激光对 316L 不锈钢微抛光效果的影响 [J]. 纳米技术与精密工程, 2011, 9(4): 370-376.
- [16] Temmler A, Liu D, Luo J, et al. Influence of pulse duration and pulse frequency on micro-roughness for

- laser micro polishing (L μ P) of stainless steel AISI 410 [J]. *Applied Surface Science*, 2020, 510: 145272.
- [17] Lü S. Study on metal micro-channel forming and quality based on nanosecond laser [D]. Guangzhou: Guangdong University of Technology, 2017: 28-29. 吕宋. 基于纳秒激光的金属微流道成型及质量研究 [D]. 广州: 广东工业大学, 2017: 28-29.
- [18] Mohajerani S, Miller J D, Tutunea-Fatan O R, et al. Thermo-physical modelling of track width during laser polishing of H13 tool steel [J]. *Procedia Manufacturing*, 2017, 10: 708-719.
- [19] Guo W K. Study on polishing DF₂ (AISI O₁) steel by Nd : YAG laser [M]//Dumitras D C. Nd : YAG laser. London: InTech, 2012: 112-134.
- [20] Liu B W, Mi G Y, Wang C M. Study on the morphology and microstructure of 5A06 alloy by high-pulse-frequency pulsed laser micro polishing [J]. *Materials Chemistry and Physics*, 2020, 255: 123500.

Pulsed Laser Polishing Mechanism on High Roughness Surface Cut by Wire Electrical Discharge Machining

Yao Jianhua^{1,2}, Huang Jinbang^{1,2}, Wang Guanghao^{1,2}, Min Dayong³, Wang Liang^{1,2*}

¹ *Institute of Laser Advanced Manufacturing, Zhejiang University of Technology, Hangzhou, Zhejiang 310014, China;*

² *Collaborative Innovation Center of High-End Laser Manufacturing Equipment Co-Sponsored by Ministry and Province, Hangzhou, Zhejiang 310014, China;*

³ *Suzhou Everbright Photonics Co., Ltd., Suzhou, Jiangsu 215000, China*

Abstract

Objective Wire electrical discharge machining (WEDM) is suitable for the cutting of various metal parts with irregular contours. Fast-speed WEDM has a lower cost and higher efficiency than lower-speed WEDM. However, the surface roughness after fast-speed WEDM is larger and generally up to $R_a = 3\text{--}6\ \mu\text{m}$. For the polishing of WEDM rough surface, the existing methods mainly include mechanical polishing, chemical polishing, and electropolishing, but they have the disadvantages of low efficiency, high manual strength, high environmental pollution, and difficulty in polishing irregular parts. Laser polishing (LP) is a new surface polishing technology, which emerged during the development of laser processing technology. It has many advantages, such as high efficiency, no pollution, selective polishing, and irregular surface polishing, thereby avoiding the disadvantages of the traditional polishing methods. Presently, research on the pulsed LP (PLP) high surface roughness and its mechanism is inadequate. In this study, the fast-speed WEDM high surface roughness of 316L stainless steel (SS) was polished with a pulsed laser; then, the surface topography before and after polishing was photographed using a microscope with a super depth of field (SDoF) by which the surface profile and roughness were measured. Finally, the evolution law of polished surface morphology and PLP mechanism under different pulse duration values and energy forms was analyzed.

Methods The experimental material was 316L austenitic SS. Before the experiment, a high surface roughness was obtained using a DK77-30 CNC WEDM machine with up to $3.79\ \mu\text{m}$ surface roughness. Then, the surface was polished with a master oscillator power amplifier (MOPA) nanosecond pulsed laser with 100 W maximum average power and $100\ \mu\text{m}$ focused-spot diameter. To prevent the surface oxidation of the material, during the LP process, the workpiece was placed in an atmosphere protection box wherein high-purity Ar was continuously supplied with a 15 L/min gas flow rate. Finally, NIKON stereoscopic and Keyence VHX-5000 microscopes with SDoFs were used to, respectively, photograph and observe the macroscopic/microscopic morphologies of the polished surface. The TR-130A surface roughness tester was used to detect the surface roughness of the sample after polishing.

Results and Discussions As shown in Fig. 4, the microscopic peaks reduced under different pulse duration values. With 10 ns pulse duration, more initial valleys remained [Fig. 3(a)], and the crater-like appearance did not disappear [Fig. 4(a)]. With 50 ns pulse duration, the number of residual valleys decreased, and only a few deep valleys remained [Fig. 3(b)]. With the subsequent increase in pulse duration, the morphology after polishing tended to be consistent [Fig. 3(c-f)], and the contour had no peak and valley but an approximately horizontal and slightly

fluctuating line [Fig. 4(g)]. As shown in Fig. 5, different pulsed laser energy forms had different effects on the surface morphology. The peaks reduced under the “low frequency with high energy” energy form, and several valleys remained [Fig. 6(a)]. Under “high frequency with low energy” energy form, valley was filled and surface morphology was smooth [Fig. 6(d)].

As shown in Fig. 7(a), the surface roughness decreased with the increase in pulse duration and was finally saturated ($R_a = 0.95 \mu\text{m}$). However, the fluctuation in a wide range of the surface was difficult to be removed, preventing the roughness from further decrease. As shown in Fig. 7(b), surface roughness gradually decreased with the energy form change from “low frequency with high energy” to “high frequency with low energy,” and the melting mechanism of “high frequency with low energy” had a more sustainable energy input and was more suitable for high surface roughness polishing. The gasification mechanism of “low frequency with high energy” was more suitable for low surface roughness polishing.

To further explore the action mechanism of pulsed laser on microscopic peak and valley of high surface roughness, a single pass experiment was conducted with different energy forms, and the change in microscopic peak and valley in the laser action area was observed using a microscope with SDoF. The “low frequency with high energy” form had a better effect on smoothing low peaks and shallow valleys than deep valleys but lacked continuous heat input and melt flow to fill deep valleys (Fig. 8). The “high frequency with low energy” form has a better effect on smoothing the microsurface topography, with continuous heat input and long-time melt flow of the material, resulting in a smooth surface (Fig. 9).

Conclusions In this study, a MOPA nanosecond pulsed laser with a wide range of adjustable pulse duration and repetition frequency was adopted to polish WEDM high roughness surface. The three-dimensional morphology, two-dimensional contour, and surface roughness of the polished surface under different pulse duration values and energy forms were analyzed. The following were observed.

1) Keeping other laser parameters constant, the microscopic surface peaks reduced under different pulse duration values, whereas the valleys showed a trend of gradually being filled as the pulse duration increased, and the surface roughness decreased from the initial $R_a = 3.79 \mu\text{m}$ to $0.95 \mu\text{m}$.

2) Keeping other laser parameters constant, with the pulse energy form change from “low frequency with high energy” to “high frequency with low energy”, the surface vaporization acting trace gradually became shallower, the peaks reduced and valleys were gradually filled, and the surface roughness decreased from the initial $R_a = 3.79 \mu\text{m}$ to $1.37 \mu\text{m}$.

3) With different energy forms, when the polishing mode gradually changed from pulsed polishing to quasi-continuous polishing, the surface polishing mechanism evolved from the gasification melting parallel polishing to simple melting polishing, and melting polishing was more suitable for polishing high roughness surface.

4) The main reason PLP could reduce the surface roughness was the smoothing effect of the narrow peaks on the surface. The macroscopic fluctuation of the initial high roughness surface could not be smooth, which limited the further decrease in roughness when the PLP used the high roughness surface.

Key words laser technique; laser materials processing; pulsed laser; laser polishing; surface morphology; surface roughness

OCIS codes 140.3390; 160.3900; 240.5450